Hindawi Publishing Corporation
EURASIP Journal on Wireless Communications and Networking
Volume 2010, Article ID 406749, 17 pages
doi:10.1155/2010/406749

Research Article

Impact of Base Station Cooperation on Cell Planning

Ian Dexter Garcia,[1] Naoki Kusashima,[1] Kei Sakaguchi,[1] Kiyomichi Araki,[1] Shoji Kaneko,[2] and Yoji Kishi[2]

[1] *Graduate School of Science and Engineering, Tokyo Institute of Technology, 2-12-1 Ookayama, Meguro-ku, Tokyo 152-8550, Japan*
[2] *Mobile and Wireless Research and Development Department, KDDI R&D Laboratories, Inc., 2-1-15 Ohara, Fujimino, Saitama 356-8502, Japan*

Correspondence should be addressed to Ian Dexter Garcia, garcia@mobile.ee.titech.ac.jp

Received 31 October 2009; Revised 24 May 2010; Accepted 10 June 2010

Academic Editor: Geert Leus

Base station cooperation (BSC) has been identified as a key radio access technology for next-generation cellular networks such as LTE-Advanced. BSC impacts cell planning, which is the methodical selection of base station (BS) sites, and BS equipment configuration for cost-effective cellular networks. In this paper, the impact of BSC on cell plan parameters (coverage, traffic, handover, and cost), as well as additional cell planning steps required for BSC are discussed. Results show that BSC maximizes its gains over noncooperation (NC) in a network wherein interference from cooperating BSs is the main limitation. Locations exist where NC may produce higher throughputs, therefore dynamic or semistatic switching between BSC and NC, called fractional BSC, is recommended. Because of interference from noncooperating BSs, the gains of BSC over NC are upper bounded, and diminishes at greater intersite distances because of noise. This encourages smaller cell sizes, higher transmit powers, and dynamic clustering of cooperative BSs.

1. Introduction

Base station cooperation (BSC) is the dynamic coordination of cellular base stations (BSs), where BSs perform cooperative transmission (CT) to user equipments (UEs) in the downlink or cooperative reception (CR) in the uplink. BSC has been proposed in numerous works, under nomenclature such as base station cooperation [1, 2]; coprocessing [3]; cooperative processing [4]; coordinated processing [5]; coordinated network [6]; coordinated beamforming [7]; distributed multicell beamforming [7]; network MIMO [8, 9]. It has been considered primarily to increase the performance of UEs with worst-case throughput. In an uncoordinated network, the poor performance of worst-case UEs is often due to strong interference from surrounding cells. For these UEs, cooperation can improve signal quality, reduce interference, and result in significant throughput gains. Recently, the 3GPP organization has been considering BSC as a primary technology candidate for 4G cellular networks [10]. Under the 3GPP technical specification [10], BSC is a category of coordinated multipoint transmission (CoMP), which is defined as the dynamic coordination among multiple geographically separated transmission points (or "geographically separated or directionally distinct transmission points" [11]). CoMP also includes the possibility for a single BS to have antennas at multiple geographically separated points without enjoying coordination from other BSs. Nevertheless, if each BS transmission point is viewed as having its own cell, then the cell plan design principles for BSC would be applicable to CoMP in general.

Meanwhile, cell planning (CP) (also known as cellular radio network planning) is the methodical selection of BS site locations and static BS equipment configuration for mobile cellular networks [12–17]. A good cell plan ensures sufficient transmission qualities and cost-effective communication service. Traditional cell plan schemes assume that BSs perform non-cooperative (NC) transmission and reception. In NC, the transmissions from each BS are independent, and the signals from other cells in the same frequency are considered as interference. Consequently, in cell planning for NC, the signal coverages are controlled to minimize coverage overlap [15]. However, when the BSs can coordinate to dynamically

reduce interference or balance loads, signal coverage overlap can be tolerated or even desired.

In cell planning of non-cooperative transmission, coverage is determined based on the area at which the required Eb/No to support a target service is met. This Eb/No is derived directly from the SINR experienced at the demodulation-decoding block of the receiver, where the interference power is taken from the sum of the in-cell interference and the total receive power from all other cells. However, this cannot be the case in base station cooperation, since signals from cooperating base stations may contain desired signal components or the interference from the cooperating base station can be cancelled at the demodulation-decoding block. Therefore, in BSC transmission, estimating the equivalent interference power as the receive power from other cells is insufficient to estimate the coverage and capacity. In this paper, two receive signal strength ratios based on reference signals are proposed: the local-to-uncooperative-plus-noise ratio (LUNR) and the local-to-cooperative-ratio (LCR). Coverage and capacity can be predicted via these ratios by expressing the spectral efficiency of BSC transmission based on these ratios.

In practical deployment, UEs at certain locations may exist where NC transmission on them yields higher spectral efficiency than BSC transmission. Therefore, in such scenarios, fractional cooperation must be performed—BSCs perform BSC transmission to UEs in some locations (called the cooperation region) while not performing BSC to UEs in the other locations (noncooperation region). In this paper, we analyze the impact of the different cooperating BS cluster types and site-to-site distances on the spectral efficiency, the area and shape of the cooperation regions, the coverage, and the capacity of the BSC network.

By understanding the impact of BSC on cell planning, a general cell planning framework applicable to a BSC network, NC network, or their hybrid network can be developed. Some discussions from this paper are based on the authors' previous papers [18, 19]. Discussion will be limited to the downlink, but the principles are extendable to the uplink. The paper organization is as follows. First, the downlink multicell transmission model will be introduced in Section 2. Second, an overview of various downlink BSC schemes and a derivation of their spectral efficiencies from their multicell receive signal strengths will be given in Section 3. Third, fractional BSC operation will be explained in Section 4. Next, impacts of cooperation on cell coverage, cell traffic, handover, cost, and complexity are discussed in Section 5, followed by its impact on cell planning procedure in Section 6. Finally, conclusions and recommendations will be stated in Section 7.

2. Downlink Multicell Transmission Model

Consider a downlink cellular network with B BSs and U user equipments (UEs, or users). All BSs have N_{T} transmit antennas each, and each UE has N_{R} receive antennas. Each BS can support an unlimited number of UEs and has no maximum limit to total capacity. The network is over a geographic area $\mathcal{A}$ with estimated propagation and service information at each called service test point (STP; or location), represented by $\mathcal{S} = \{S_1, S_2, \ldots, S_{N_S}\}$, where N_S is number of STPs in $\mathcal{A}$ and S_s denotes STP s.

2.1. Channel Model. The average amplitudes of the BS-to-UE links are in $\mathbf{A} \in \mathfrak{R}^{U\times B}$, whose matrix elements are $\alpha_{u,b}$. For each resource slot, the multicell channel is expressed as

$$\mathbf{H} = \left[\mathbf{A} \otimes \mathbf{1}_{N_{\mathrm{R}}\times N_{\mathrm{T}}}\right] \circ \widetilde{\mathbf{H}}, \tag{1}$$

where $\otimes$ and $\circ$ denote matrix Kronecker product and Hadamard product, respectively, and $\mathbf{1}_{N_{\mathrm{R}}\times N_{\mathrm{T}}}$ is an $N_{\mathrm{R}} \times N_{\mathrm{T}}$ matrix of ones. $\widetilde{\mathbf{H}} \in \mathfrak{C}^{N_{\mathrm{R}}U\times N_{\mathrm{T}}B}$ whose block elements vary according to the link-by-link MIMO spatial small-scale fading models (e.g., Kronecker model, etc.). The total channel to UE u is $\mathbf{H}_u$ which contains $\mathbf{H}_{u,b}$ from BSs $b = 1, \ldots, B$.

2.2. BS Categories. From the viewpoint of each UE, there are three categories of BSs. The first is the *local BS* (also commonly called anchor BS, home BS, or serving BS). The local BS governs the transmission to a group of UEs. This means that it decides which BS or BSs can transmit data to these UEs and the manner of transmission (i.e., link adaptation mode). The second are the *cooperative BSs*, which are the BSs that can cooperate with the local BS and are in the same BSC *cluster*. The third are the *non-cooperative BSs*. The selection of BSs within each category can be dynamic over time and frequency.

The average power of the received signal at the UE u at a location S_s from its local BS of the BSC cluster k is $L_u(s) = P_{l_u}\alpha^2_{(s),l_u}$, where l_u denotes the index of the local BS of UE u and P_{l_u} is the total transmit power of BS l_u. Similarly, the average power of the received signals from cooperative BS a_u is $C_{u,a}(s) = P_{a_u}\alpha^2_{(s),a_u}$; and average power from uncooperative BS f_u is $U_{u,f_u}(s) = P_{f_u}\alpha^2_{(s),f_u}$.

Typically, the "cell" of a BS b is chosen as

$$\mathcal{C}_b = \left\{S_s : L_{(s),b} > L_{\mathrm{STR}}; L_{(s),b} \geq L_{(s),i}\ \forall i \neq b\right\} \quad (\text{cell } b), \tag{2}$$

where $L_{(s),b}$ is the receive signal strength of a UE at S_s from BS b and L_{STR} is the signal strength service threshold requirement.

2.3. BSC Set Clusters. In a multicell network with a large number of cells, practically speaking, only a small number of BSs can perform BSC transmission or BSC reception with each other simultaneously. Moreover, beyond a small number that depends on the network geometry, the relative gain of increasing the cluster size diminishes since the signal from other BSs are much weaker than others, as confirmed in [9]. Hence, a large multicell network must be divided into static cooperative BS clusters, or a dynamic clustering of BS must be performed. Both are cases of a *partial BSC network* (or groupwise BSC network), as opposed to a *full BSC network* where all BSs cooperate simultaneously.

The BSs are grouped into K BSC clusters, with each cluster having $B_{\mathrm{C},k}$, $(k = 1, \ldots, K)$ BSs. On the other

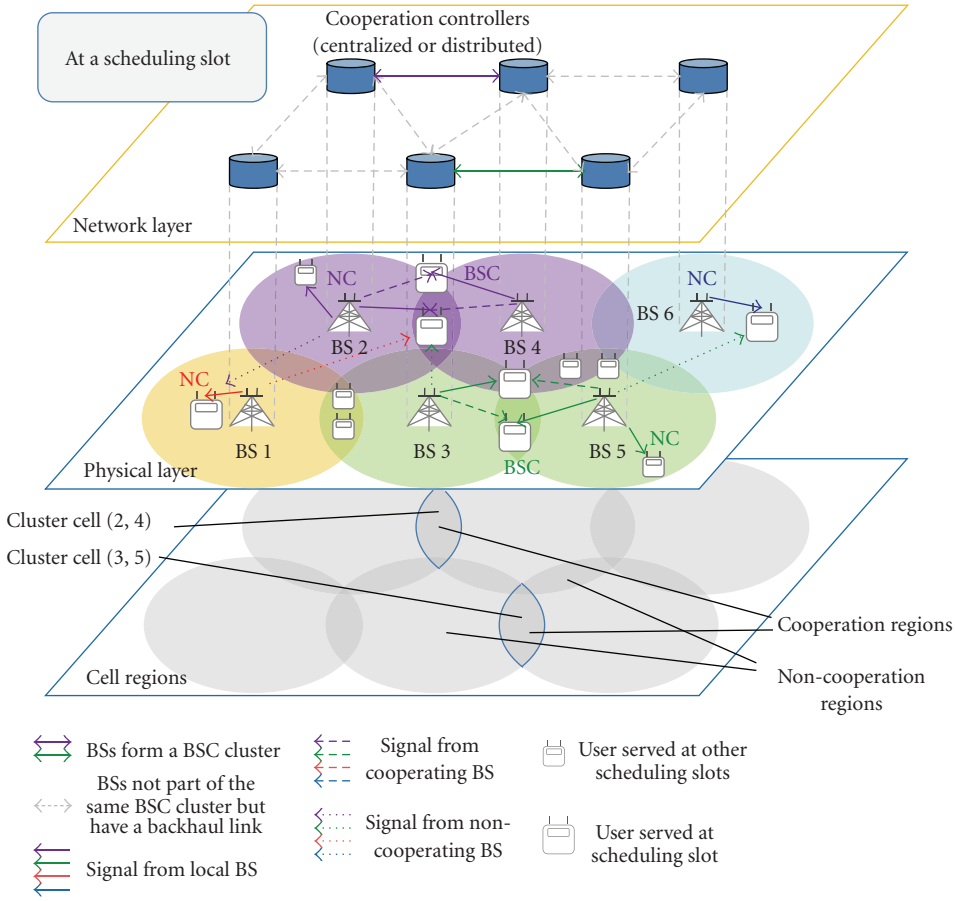

Figure 1: Fractional BSC cellular network.

hand, the stations of other clusters are independent and behave as interferers to these UEs. Each cluster is named Cluster $(x, y, z, \ldots)$, where x, y, and z are the indices of the cooperating BSs, and has a corresponding *cluster cell* region. This means that any or all BSs of the cluster directly transmit or receive information from UEs within its cluster cell.

There are $U_{C,k}$ simultaneously scheduled UEs within the kth cluster. UE u of the kth Cluster receives d_{u_k} parallel information streams. Information streams of UE u of cluster k are denoted by $\mathbf{d}_{u_k} \in \mathfrak{C}^{v_{u_k}}$ where v_{u_k} is the number of its information streams and each element is unit power on average. These may be shared by the cooperation cluster BSs and jointly processed through a weighting matrix $\mathbf{T}^{(k)} \in \mathfrak{C}^{B_{C,k} t \times \sum v_{u_k}}$.

Under NC, throughput of the uth UE may be estimated from the received signal power ratio

$$\mathrm{LUCNR}_u \triangleq \frac{L_u}{\left(\sum_f U_{u,f_u} + \sum_a C_{u,a_u} + N\right)} \tag{3}$$

which is referred to as the local-to-uncooperative-plus-cooperative-plus-noise ratio (LUCNR). It is also referred to as the geometry factor, or G-factor in other texts. Here, N is the power of the noise including the noise figure.

Similarly under BSC, the throughput of the uth UE may also be estimated from its receive signal strength ratios such as

$$\mathrm{LNR}_u \triangleq \frac{L_u}{N} \quad \text{local-to-noise ratio (LNR)},$$

$$\mathrm{LUR}_u \triangleq \frac{L_u}{\left(\sum_f U_{u,f_u}\right)} \quad \text{local-to-uncooperative ratio (LUR)},$$

$$\mathrm{LCR}_{u,a_u} \triangleq \frac{L_u}{C_{u,a_u}}, \qquad \mathrm{LCR}_u \triangleq \frac{L_u}{\left(\sum_{\forall a_u} C_{u,a_u}\right)}$$

$$\text{local-to-cooperative ratio (LCR)},$$

$$\mathrm{LUNR}_u \triangleq \frac{L_u}{\left(\sum_f U_{u,f_u} + N\right)}$$

$$\text{local-to-uncooperative-plus-noise ratio (LUNR)}. \tag{4}$$

If the UE has no prior knowledge of signals from the uncooperative BSs, the total interference signal from uncooperative BSs can be conservatively treated as uncorrelated AWGN with received power $U_u = \sum_{f_u} U_{u,f_u}$. This realistic assumption is used in the succeeding discussions.

2.4. Cell Regions. Each cell area may be divided into cell regions according to the received signal strength profile at each location, as shown in Figure 2:

$$\begin{aligned}
&\mathcal{CI}_b \triangleq \left\{S_s \in \mathcal{C}_b : \mathrm{LUCNR}_{(s)} \geq \mathrm{LUCNR}_{\mathrm{edge}}\right\} \quad \text{(cell-inner)},\\
&\mathcal{CE}_b \triangleq \left\{S_s \in \mathcal{C}_b : \mathrm{LUCNR}_{(s)} < \mathrm{LUCNR}_{\mathrm{edge}}\right\} \quad \text{(cell-edge)},\\
&\mathcal{CE}_{\mathrm{intra},b} \triangleq \left\{S_s \in \mathcal{C}_b : \mathrm{LUCNR}_{(s)} < \mathrm{LUCNR}_{\mathrm{edge}}, C_{(s)} \geq U_{(s)} + N\right\}\\
&\text{(intracluster cell-edge)},\\
&\mathcal{CE}_{\mathrm{inter},b} \triangleq \left\{S_s \in \mathcal{C}_b : \mathrm{LUCNR}_{(s)} < \mathrm{LUCNR}_{\mathrm{edge}}, C_{(s)} < U_{(s)} + N\right\}\\
&\text{(intercluster cell-edge)},
\end{aligned} \tag{5}$$

where $\mathrm{LUCNR}_{\mathrm{edge}}$ is an arbitrary value but is usually set below 10 dB. The intercluster cell-edge is also referred as the cluster-edge.

In addition, the regions may be subdivided according to LNR:

$$\begin{aligned}
&\mathcal{SI}_b \triangleq \left\{S_s \in \mathcal{C}_b : \mathrm{LNR}_{(s)} \geq \mathrm{LNR}_{\mathrm{edge}}\right\} \quad \text{(site-inner)},\\
&\mathcal{SE}_b \triangleq \left\{S_s \in \mathcal{C}_b : \mathrm{LNR}_{(s)} < \mathrm{LNR}_{\mathrm{edge}}\right\} \quad \text{(site-edge)},
\end{aligned} \tag{6}$$

where $\mathrm{LNR}_{\mathrm{edge}}$ is also arbitrary and is usually set to a low dB value.

2.4.1. BSC Cluster Types. Each BSC cluster can be categorized as either intrasite, intersite, or hybrid.

In an *intrasite BSC cluster*, cooperation is limited to within cells of the same BS in one site. Intrasite CoMP allows a site to overcome the backlobe interference caused by the other cells within the same site. Cooperation does not require a high-speed, low-latency, intersite backhaul connection. If the BSs of the site can coordinate all of its cells, then the BSC cluster size is the same as the number of cells on the site, and the clustering of transmission points as a BSC cluster remains static. In an *intersite BSC cluster*, cooperation is limited only to within cells of different sites. This method addresses the interference problem at the site-edge. However, this does not address the antenna backlobe interference from the other cells within the same site. In intersite BSC, cooperation requires a high-speed, low-latency, intersite backbone connection. Intrasite and intersite clusters are illustrated in Figure 3 with the approximate cell region locations for a three-sector/site hexagonal cell pattern.

In a *hybrid BSC cluster*, the cooperation set is composed of at least one transmission point from another site and at least one transmission point from the same site.

2.4.2. Static and Dynamic Clustering. Under *static clustering*, the cooperative BS clusters remain fixed. Under *dynamic clustering*, cooperative clusters periodically regroup. An example criterion of dynamic clustering is to form clusters such that as much as possible, the strongest signals received by each UE are from the serving cluster.

In *agile dynamic clustering*, the network intelligently switches between intrasite, intersite, and hybrid BSC clusters in order to select the best possible BSC cluster for the UE. Agile dynamic clustering and the approximate locations of its cell regions are illustrated in Figure 3. As observed, under agile dynamic clustering, the intercluster cell-edge are replaced by the intracluster cell-edges.

Figure 4 illustrates the impact of clustering and site-to-site distance on the received signal strength ratios. Since the network geometry and transmit powers are constant, the LUR and LCR CDFs are the same across varying intersite distances. At low intersite distances (e.g., 500 m), the LNRs were much higher than the LUR and LCR which made the network interference limited. Under this interference-limited network, performance primarily is dependent on the relationship of the LURs to the LCRs. Unless the LURs and LCRs change, the network performance remains the same even if transmit powers are increased. On the other hand, at high intersite distances (e.g., 3000 meters intersite distance), the LURs and LCRs for various cluster types are much higher than the LNR. Therefore, this network is primarily noise limited, and altering the LURs and LCRs should not affect the network performance significantly.

It is observed that for the test network, LUR increased and LCR decreased in going from intersite static clustering, to hybrid static clustering, to intersite dynamic clustering, and to agile dynamic clustering. In addition, an increase in the LUR corresponded to a decrease in LCR since other BSs are either cooperative or uncooperative.

2.5. Spectral Efficiency. By incorporating nonidealities, the instantaneous achievable spectral efficiency of UE u in cluster k under linear transmit precoding can be approximated as

$$R_{u_k} = \min\left\{\hat{R}_{u_k}, R_{\max}\right\} \tag{7}$$

with

$$\hat{R}_{u_k} \approxeq \chi \log_2 \left| \mathbf{I} + \frac{1}{\rho} \frac{\mathbf{H}_{u_k} \mathbf{T}_{u_k}^{(k)} \mathbf{T}_{u_k}^{(k)H} \mathbf{H}_{u_k}^H}{(N + U_{u_k})\mathbf{I} + \mathbf{H}_{u_k}\left(\sum_{i \neq u} \mathbf{T}_i^{(k)} \mathbf{T}_i^{(k)H}\right)\mathbf{H}_{u_k}^H} \right|, \tag{8}$$

where $(\cdot)^H$ is the Hermitian transpose, $\mathbf{T}_u^{(k)}$ is the uth block column of $\mathbf{T}^{(k)}$ which contain the weighting matrices for the information streams of UE u within cluster k, and $|\cdot|$ denotes the determinant. χ, $(\chi \leq 1)$, denotes the bandwidth inefficiency due to control channels, dedicated channels, pilot carriers, cyclic prefixes, guard bands, guard intervals, and so forth. ρ, $(\rho \geq 1)$, represents the SINR gap to capacity which is due to the nonoptimality of the modulation and coding scheme (MCS), precoding granularity, CSI error, CSI feedback delay, synchronization errors, pilot power allocation, cyclic prefix power allocation, and so forth. $\hat{R}_{u_k}$ is the unbounded spectral efficiency and $R_{\max}$ is the maximum user spectral efficiency which depends on the number of parallel streams, the MCS, and bandwidth inefficiency. For example, system-level spectral inefficiencies based on the downlink of the LTE and proposed LTE-Advanced standards

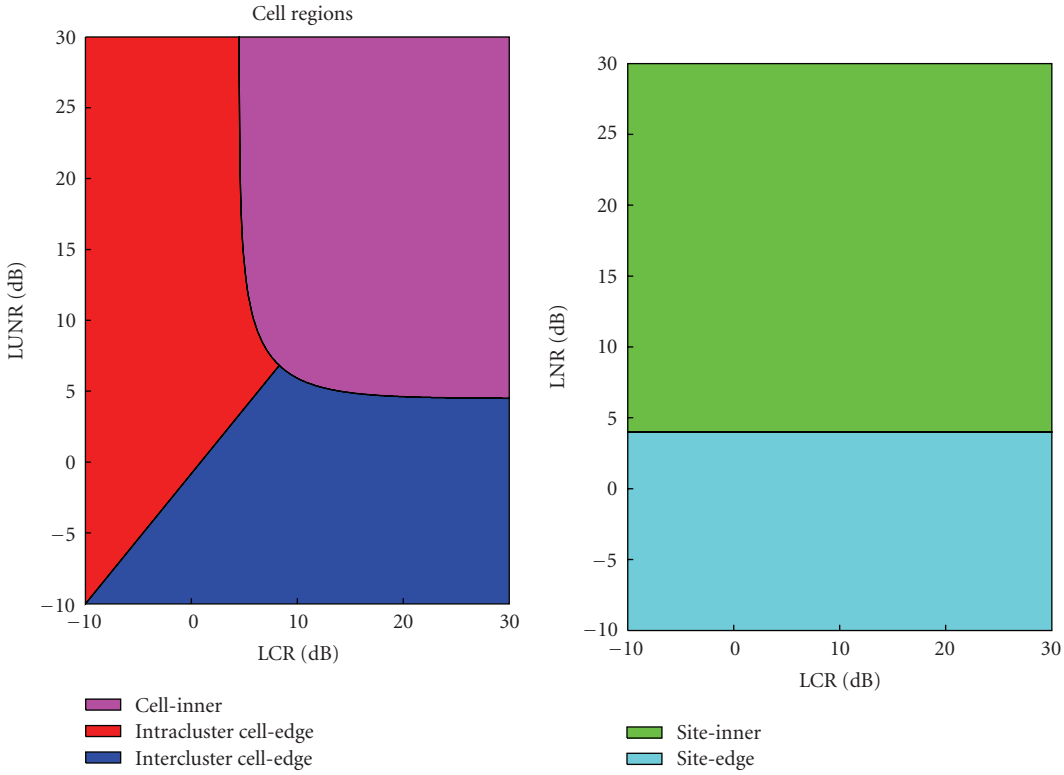

FIGURE 2: Cell region illustration. In this example, $\text{LNR}_{\text{edge}} = 4$ dB and $\text{LUCNR}_{\text{edge}} \approx 7$ dB.

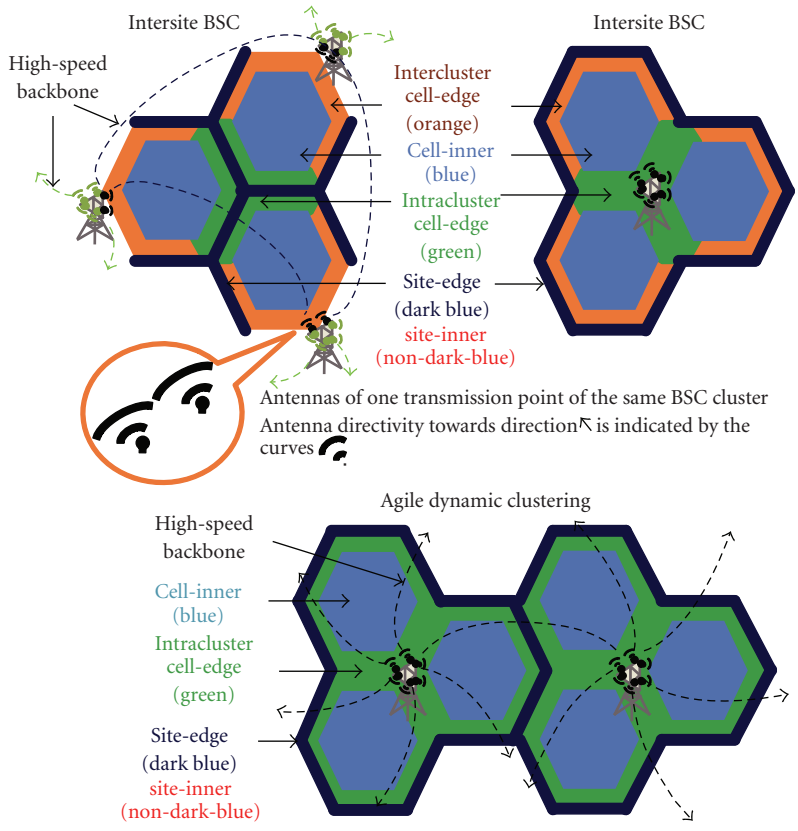

FIGURE 3: BSC cluster types and their corresponding cell regions.

Table 1: Static network parameters of the example multicell network.

Parameters	Values
Number of sites	27
Number of sectors (Cells) per Site	3
Number of UEs per cell	10
Cell shape	Hexagonal
Carrier frequency	2 GHz
No. of BS antennas, N_T	4
No. of UE antennas, N_R	2
BSC cluster Size, B_C	3
Tx power (all BSs), P	36 dBm/MHz
UE noise power, N_0	−102 dBm/MHz
Shadow fading standard deviation	6 dB
Shadow fading intersite correlation	0.5
Shadow fading intrasite correlation	1
Distance-dependent pathloss	3GPP Urban Macro NLOS $34.6078 + 35.7435\log_{10}(d_{\text{meters}})$
Penetration loss	9 dB (car penetration)
Small-scale fading	I.I.D. Rayleigh
UE antenna type (gain)	Omnidirectional (0 dB)
BS antenna type (azimuth gain) 3 sector/site	$\delta_{\text{dB}}(\theta) = 14 - \min(12\theta/70^\circ, 25)$
minimum BS-to-UE distance	$\frac{35 d_{\text{site-site}}}{500}$ meters
NC precoding	NC-SVD (Equal stream power; Per-base-power constraint)
BSC precoding	BSC-BD-SVD (Equal stream power; Per-base-power constraint)
NC Scheduling	Round-robin
NC scheduling	Round-robin inside noncooperation region
BSC scheduling	Round-robin of UE groups inside cooperation region
CSI and Synchronization errors	Modeled as implementation losses in Table 2
Link Mean Spectral Efficiency STR, $\overline{R}_{A,STR}$	1 bps/Hz

are listed in Table 2 and will be used in the succeeding simulations [20, 21].

2.6. Noncooperative Transmission. In NC transmission, signals from all surrounding BSs are regarded as purely interference. Without successive intracluster interference cancellation at the UE and an AWGN approximation of the interference, capacity is obtained in NC single-user transmission using singular value decomposition (NC-SVD) with waterfilling. The approximate achievable instantaneous user spectral efficiency for NC-SVD is

$$\hat{R}_{\text{NC-SVD},u} \cong \chi_{\text{NC}} \log_2 \left| \mathbf{I} + \text{LUNR}_u \frac{\widetilde{\mathbf{H}}_{u,b_u} \mathbf{V}_u \mathbf{P}_u \mathbf{V}_u^H \widetilde{\mathbf{H}}_{u,b_u}^H}{\rho_{\text{NC}} P_{b_u}} \right|, \tag{9}$$

where $\mathbf{P}_u$ is the stream power allocation matrix, $\text{trace}(\mathbf{P}_u) = P_u$, and $\mathbf{V}_u$ is the right-SVD matrix of the channel $\widetilde{\mathbf{H}}$. Equation (9) shows that to increase user throughputs, noncooperation encourages higher LUNR.

3. Downlink BSC Schemes

BSC schemes can be categorized according to the CoMP categorization in [10], as in the succeeding.

3.1. Coordinated Scheduling/Coordinated Beamforming. Under coordinated scheduling and/or coordinated beamforming (CS/CB), data to a UE is instantaneously transmitted from a single transmission point. Scheduling decisions are coordinated to control, for example, the interference generated in a set of coordinated cells. CS/CB does not require information stream exchange and symbol-level inter-BS synchronization.

3.2. Joint Processing (JP). Under JP, data to a single UE is simultaneously transmitted from multiple transmission points, for example, to (coherently or noncoherently) improve the received signal quality or actively cancel interference for other UEs. With proper design and synchronization, coherent joint transmission can achieve the highest possible spectral efficiency among different BSC techniques because the signals from the other sites can be used to improve the signal quality rather than reduce it. Therefore, the focus of our analysis is on coherent joint transmission.

3.2.1. Coherent Joint Transmission (JT). A canonical example of coherent joint transmission is block diagonalization with SVD (BSC-BD-SVD), where intracluster interference is

Table 2: Spectral efficiency losses based on [20, 21].

Parameters	Values
Cyclic prefix loss χ_{CP}	$\frac{14336}{15360}$
Guard band loss χ_{GB}	0.9
NC Overhead loss χ_{NCO}	$\frac{57872}{84000}$
BSC Overhead loss χ_{BSCO}	$\frac{51872}{84000}$
NC-SVD Bandwidth Ineff., $\chi_{NC-SVD} = \chi_{CP}\chi_{GB}\chi_{NCO}$	0.5787
BSC-BD-SVD Bandwidth Ineff., $\chi_{BD-SVD} = \chi_{CP}\chi_{GB}\chi_{BSCO}$	0.5187
Modulation and Coding SINR Gap to Capacity, ρ_{MCS}	2 dB
*NC-SVD Implementation Gap to Capacity, $1/\rho_{NC\text{-}Impl}$	1.9179 dB
*BSC-BD-SVD Implementation Gap to Capacity, $1/\rho_{BSC\text{-}Impl}$	2.3928 dB
NC-SVD SINR Gap to Capacity $\rho_{NC} = \rho_{MCS}\rho_{NC\text{-}Impl}$	3.9179 dB
BSC-BD-SVD SINR Gap to Capacity $\rho_{BD-SVD} = \rho_{MCS}\rho_{BSC\text{-}Impl}$	4.3928 dB
Max. subcarrier spec. eff. per symbol	$\frac{6 \times 948}{1024}$
NC-SVD Max. Spec. Eff., $R_{NC\text{-}SVD,max}$	6.4292
BSC-BD-SVD Max. Spec. Eff., $R_{BD\text{-}SVD,max}$	5.7626

*It is assumed that the energy per resource element of the control channel and reference signals are the same with the data channel. No power boosting of the control channel is performed. Also includes CSI estimation errors and precoding quantization.

eliminated. In terms of LCR and LUNR, the instantaneous achievable spectral efficiency is

$$\hat{R}_{BD\text{-}SVD,u} \cong \chi_{BD\text{-}SVD}\log_2\left|\mathbf{I} + \mathrm{LUNR}_u\beta\left(\mathbf{G}^T\mathbf{G}\otimes\mathbf{1}_{N_T\times N_T}\right)\circ\boldsymbol{\Upsilon}\right|, \tag{10}$$

where

$$\boldsymbol{\Upsilon} = \frac{\tilde{\mathbf{H}}_{u,b_u}^H\tilde{\mathbf{H}}_{u,b_u}\mathbf{Q}_{BD,u}\mathbf{V}_{BD,u}\mathbf{P}_u\mathbf{V}_{BD,u}^H\mathbf{Q}_{BD,u}^H}{\rho_{BD\text{-}SVD}P_{b_u}},$$
$$\mathbf{G}_u = \left[\frac{1}{\sqrt{\mathrm{LCR}_{u,1}}}\quad\frac{1}{\sqrt{\mathrm{LCR}_{u,2}}}\quad\cdots\quad\frac{1}{\sqrt{\mathrm{LCR}_{u,B_C}}}\right], \tag{11}$$

where β, ($\beta \le 1$), is the power normalization factor under the per-base constraint. $\mathbf{Q}_{BD,u}$ are the orthonormal null-space vectors of $\dot{\mathbf{H}}_u$ and $\mathbf{V}_{BD,u}$ is the right SVD matrix of the equivalent channel $\tilde{\mathbf{H}}_u\mathbf{Q}_{BD,u}$.

In BSC-BD-SVD, the LCRs and LUNRs of the other presently scheduled UEs affect the value of $\mathbf{Q}_{BD,u}$, and consequently the user spectral efficiencies. The optimum selection of scheduled UE groupings is a topic for future study. For theoretical evaluation, it is assumed that the cluster UEs with nearly the same LCR and LUNR values are jointly scheduled. Under a joint scheduling method, the transmission power mismatch at BSs is minimized, which increases spectral efficiencies. It is also assumed that the transmissions are perfectly synchronized so that coherent combining of signals are achieved at the UE antennas, which is required in forming the block-diagonalization nulls.

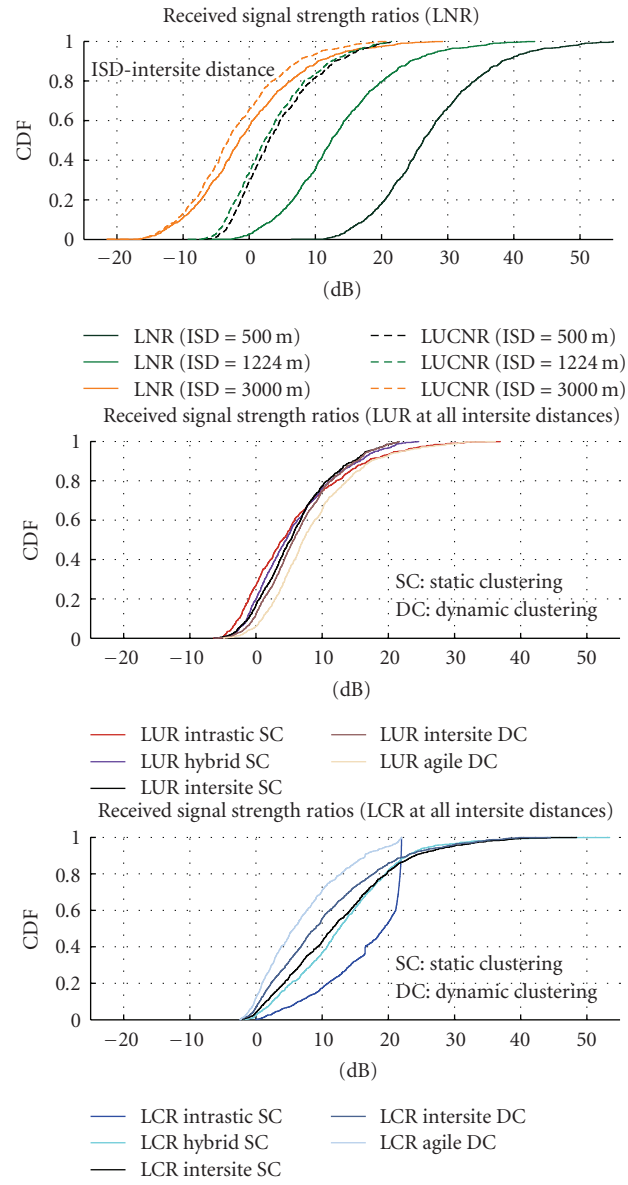

Figure 4: CDF of receive signal strength ratios under different cluster types. Simulation assumptions are in Table 1. 3-BS cooperation. Shadow fading is included.

We define the link mean spectral efficiency as the mean spectral efficiency of each BS when a single UE per cell is served. Figure 5 shows the approximate link mean spectral efficiencies of BSC-BD-SVD and NC-SVD under per-base-power constraint in linear scale and logarithmic scale. In this figure, it is assumed that some of the BSs can perform both NC-SVD and BSC-BD-SVD. Under NC, the BSs assigned as "cooperative" still transmit interference signals. For NC-SVD, it is observed that the spectral efficiency increases monotonically with respect to LUNR and LCR, since the signals from any other BS are purely interference. However, for BSC-BD-SVD, its surface shows that there is a depression at around $\mathrm{LCR}_u = 0$ dB. This means that when the signals from the cooperative BSs are about as strong as that of the local BS, gains in spectral efficiency can be obtained

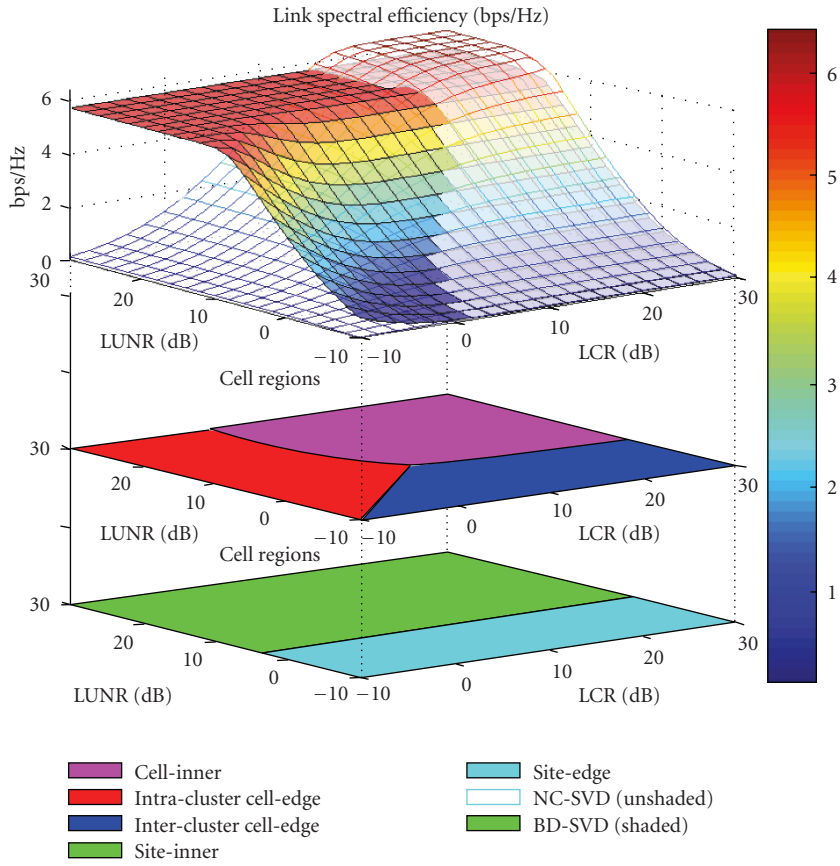

Figure 5: Link mean spectral efficiencies of NC-SVD and BSC-BD-SVD under 4×2 MIMO, $B_C = 3$, I.I.D. Rayleigh fading, equal stream powers, and spectral efficiency losses are listed in Table 2. The two surfaces are superimposed. The bottom two subfigures show the corresponding cell regions illustrated in Figure 2.

by further increasing the receive signal strength from the cooperative BSs. In the top subfigure, the absolute effect of BSC to spectral efficiency is shown. At high LUNR, the contribution of BSC is in the order of several bps/Hz, and at very low LUNR, the contribution is in the order of 10^{-1}–10^{-2} bps/Hz. Therefore, in the absolute sense, at high LUNR, the contribution of BSC is high, and at low LUNR, the contribution of BSC is low.

On the other hand, when the spectral efficiencies are viewed in the logarithmic scale, under the same LUNR, the relative effect of LCR to spectral efficiency is observed. We see that the LCR value has a more noticeable effect on the relative spectral efficiency at low LUNR. At low LUNR, the change in spectral efficiency for varying LCRs can be up to one decade, while at high LUNR, the change is much less. This means that at low LUNR, the relative contributions of cooperating BSs on the spectral efficiency is significant. Conversely, at high LUNR, the relative contribution of the cooperating BSs is small.

Because of the bandwidth modulation and coding limitations, the spectral efficiencies have limits at high LUNR values, with BSC-BD-SVD having a limit that is less than that of NC-SVD because of the added pilot subcarriers required to estimate the CSI of the multicell channels. Therefore, NC achieves higher instantaneous spectral efficiency at high LUNR and LCR environments.

Figure 5 also indicates the spectral efficiencies at the different cell regions. At the site-edge, since LNR is small, LUNR is also small. Even if BSC is performed, the spectral efficiency remained low. To increase the spectral efficiency at the site-edge locations, transmit power must be increased, in addition to performing BSC. At the cell-inner, NC-SVD showed spectral efficiency gains over BSC-BD-SVD. At the intercluster cell-edge, the spectral efficiency remained low even with cooperation, since the intercluster interference with noise is dominant over the intracluster signals. However, at the intracluster cell-edge, the spectral efficiency of BSC can increase significantly over that of NC especially at high LUNR, as indicated in Figure 5.

4. Fractional BSC

In a fractional BSC network (FBSC network), the BS dynamically or semistatically selects NC or BSC transmission to each UE based on the transmission scheme that would maximize the instantaneous or mean throughput, or some other criterion. For the case where average spectral efficiency is maximized semistatically,

$$\overline{R}_{\text{mix},u} = \max\left(\overline{R}_{\text{NC},u}, \overline{R}_{\text{BSC},u}\right). \tag{12}$$

Since fractional BSC affords the highest possible spectral efficiency at every cell location, the cell-average and 5% cell-edge spectral efficienies of fractional BSC are higher than both of BSC and NC. In effect, two cell regions are formed based on the LUNR and LCR, as shown in Figure 5. These are

$$\mathcal{CR} \triangleq \left\{S_s : \overline{R}_{\mathrm{BSC},(s)} \geq \overline{R}_{\mathrm{NC},(s)}\right\} \quad \text{(cooperation region)},$$
$$\mathcal{NCR} \triangleq \left\{S_s : \overline{R}_{\mathrm{BSC},(s)} < \overline{R}_{\mathrm{NC},(s)}\right\} \quad \text{(noncooperation region)}. \tag{13}$$

An FBSC network is illustrated in Figure 1.

4.1. Impact of Clustering on UE Spectral Efficiencies. By mapping the joint PDFs of Figures 5 and 6, the impact of clustering on UE spectral efficiencies, as shown in Figure 7, can be examined. For intrasite clustering, the LCR was mostly around 20 dB, where there is no gain of BSC over NC. In addition, there was a low concentration at the cell-edge region (low-LUNR low-LCR region). Therefore, the 5% mean user spectral efficiency of BSC-BD-SVD under intrasite clustering was lower than for noncooperation. However, there was a slight concentration of users in the low-LCR, high-LUNR region, which are the locations at the borders of the sectors at the site-inner. This led to relatively higher spectral efficiency for the top 25% of users compared to NC, as indicated in the CDF.

For static intersite clustering, there was a larger concentration of UEs in the cell-edge region compared to intrasite clustering. For BSC-BD-SVD, this led to better 5% mean user spectral efficiency, compared to intrasite clustering. However, the top 25% of users experienced a reduction in spectral efficiency compared to intrasite clustering since the LCRs were mostly high at the high LUNR region. By performing dynamic intersite clustering, a concentration at the lower LCRs was experienced, which led to higher spectral efficiency compared to static clustering. However, the LUNRs were still generally lower than the LCRs, which means that the network was still primarily intercluster interference and noise limited. By performing agile dynamic clustering, the LCRs were reduced to generally lower than the LUNRs, which maximized the impact of cooperation on spectral efficiency. Further gains in spectral efficiency were realized through fractional cooperation.

4.2. Impact of Clustering Type on Cooperation Region Area. Consider the following network example under Tables 2 and 1 assumptions. The site locations, and cluster cell $\mathcal{C}^{\mathrm{static}}_{(3,4,8)}$, under static clustering, no shadowing, and 500 meters intersite distance are shown in Figure 8. It is observed that the cooperation region was around 30% of the cluster cell area. For 70% of the cell cluster area, which includes the cell-inner and intercluster cell-edge, BSC-BD-SVD performed worse than NC-SVD.

The cooperation regions for the other cluster types are shown in Figures 9 and 10. When compared with Figure 3, it is observed that the cooperation regions were around the intracluster cell-edges. It is also observed that for the test network, the cooperation region increased in going from intrasite static cluster, to hybrid static cluster, to intersite static cluster, to intersite dynamic cluster, and to agile dynamic cluster. This trend for the cooperation region ratio correlates with the trend observed in Figure 4, wherein the LUR increases and LCR decreased under the same ordering. By increasing the LURs and decreasing the LCRs, the area at which BSC achieves gains increases.

When agile dynamic clustering was performed, the cooperation region became around 80% of the cell area, which is much larger than that of static clustering. Each cluster cell became limited to a smaller area, and there were more possible cluster combinations. For example, different cluster cells are shown in Figure 10.

4.3. Impact of Intersite Distance on Cooperation Region Area. The relative areas of the cooperation region for varying intersite distance are shown in Figure 11. It is observed that at a sufficiently high intersite distance, the cooperation region almost disappears since the LNRs are lower, which limit the gain of cooperation. The results also show that the ratios saturated at low intersite distances. This is because at low intersite distances, the received signals are primarily intercluster interference limited, which are also not addressed by the cooperation. A larger cell area experienced spectral efficiency gain through BSC by using intersite BSC over intrasite BSC. Agile dynamic clustering resulted in the largest cooperation region.

5. BSC Impact on Cell Planning Parameters

5.1. BSC Impact on Coverage. For noncooperation, it is easy to estimate the SINR level by directly using L_u, C_u, U_u, and N_0. However, for cooperation, the equivalent interference level is dependent on the method of cooperation. Moreover, as stated in the introduction, BSC is being considered primarily to increase the worst-case user spectral efficiencies. Therefore, it is reasonable to estimate the service threshold directly through spectral efficiency. A threshold link mean user spectral efficiency may be used as a coverage threshold.

Given a spectral efficiency requirement $\overline{R}_{\mathrm{STR}}$ and the set of STPs, the spectral efficiency coverage optimization problem is as follows.

Spectral Efficiency Coverage Optimization. It holds that

$$\begin{aligned} &\text{maximize} \quad \mathbb{V}_{\mathrm{SE}} = N_{\mathbb{V}_{\overline{R}}} \\ &\text{such that} \quad N_{\mathbb{V}_{\overline{R}}} = \sum_{s=1}^{N_S} \iota_s \\ &\qquad \iota_s = \begin{cases} 1 & \overline{R}_{(s)} \geq \overline{R}_{\mathrm{STR}} \\ 0 & \text{otherwise}, \end{cases} \end{aligned} \tag{14}$$

where $\mathbb{V}_{\mathrm{SE}}$ is the spectral efficiency coverage metric.

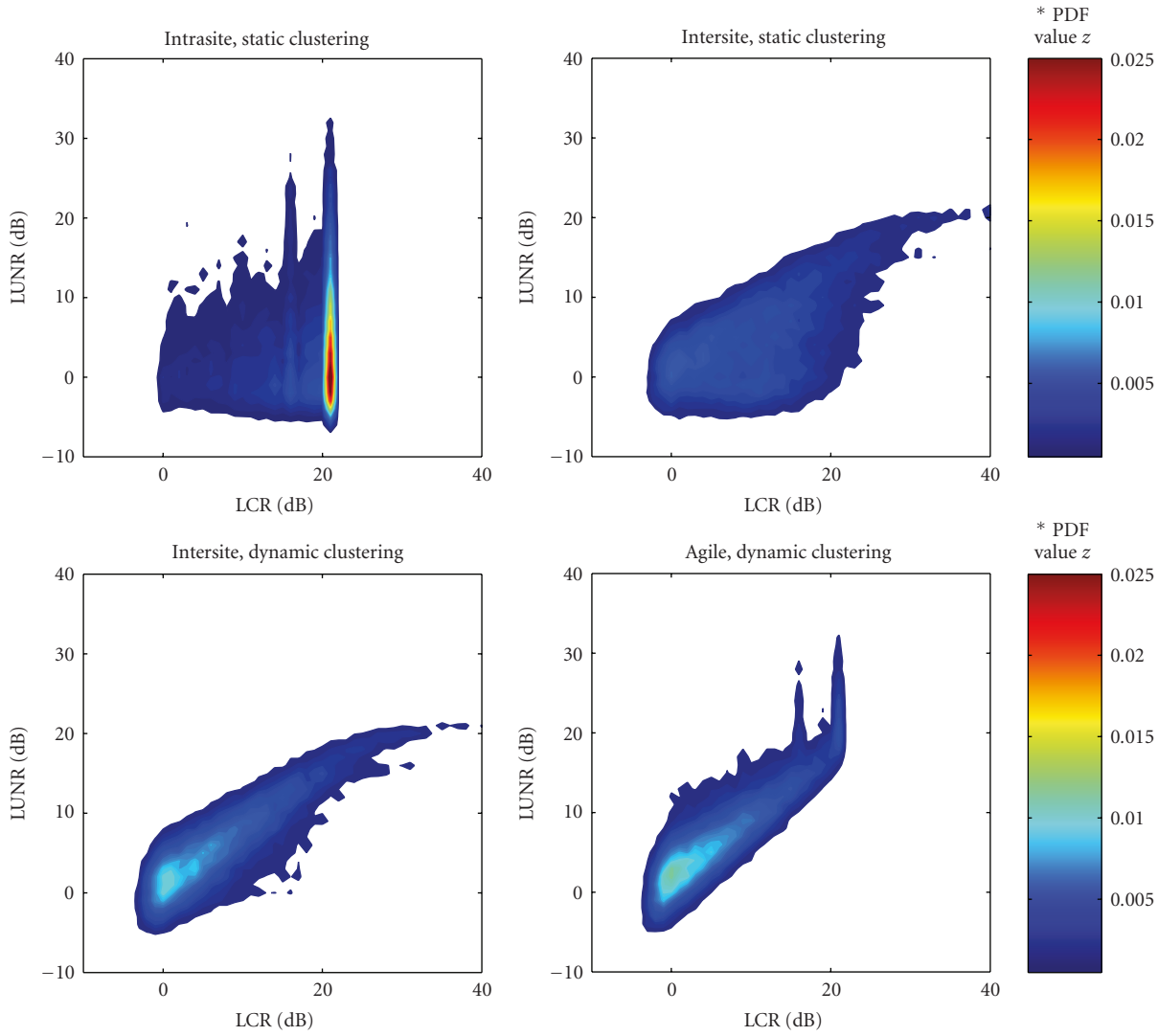

Figure 6: Joint PDF of UE receive signal strength ratios under different clustering schemes. $^{*}z = p(x-1 \leq \mathrm{LCR}_{\mathrm{dB}} < x, y-1 \leq \mathrm{LUNR}_{\mathrm{dB}} < y)$. Simulation assumptions are in Table 1. 3-BS cooperation. Shadow fading is included. 500 m site-to-site distance.

To understand the effect of cooperation on signal power and spectral efficiency coverage, let us estimate the worst-case link mean spectral efficiency of the test network for NC-SVD under no shadow fading. Because there is no shadow fading, the achievable spectral efficiency of NC-SVD is lowest at the corner of each cell boundary. Along the boundary, two locations of interest are studied. The 1st is "Location 1," where the LCR is highest among other cell boundary locations. Location 1 belongs to the intercluster cell-edge. The 2nd is "Location 2," where the LCR is lowest among other cell boundary locations. Location 1 belongs to the intracluster cell-edge. Both locations are shown in Figure 8.

The link mean user spectral efficiencies of Locations 1 and 2 under no shadowing are shown in Figure 12 under varying intersite distance. It is observed that the spectral efficiencies under NC-SVD were nearly identical for both locations since the signal strengths ratios were nearly identical in both locations. There was a saturation as the intersite distance dropped below 1000 meters where interference has a dominant effect over the noise (i.e., reducing intersite distance or increasing transmit power does not necessarily increase worst-case spectral efficiency). For this range of values, we say that the achievable spectral efficiency is interference limited, and differentially decreasing the intersite distance or differentially increasing all the BS transmit powers does not improve the cell-edge spectral efficiency. This phenomenon illustrates the fundamental limitation of NCT networks at the cell-edge.

BSC-BD-SVD under static clustering resulted in different perfomance between Locations 1 and 2. In Location 1, cooperation yielded even lower spectral efficiency compared to that of NC-SVD. This is because the loss in the allocated power for the UE at Location 1 by BS 1 counterbalanced the small gain in capacity from the cooperative BSs. The huge

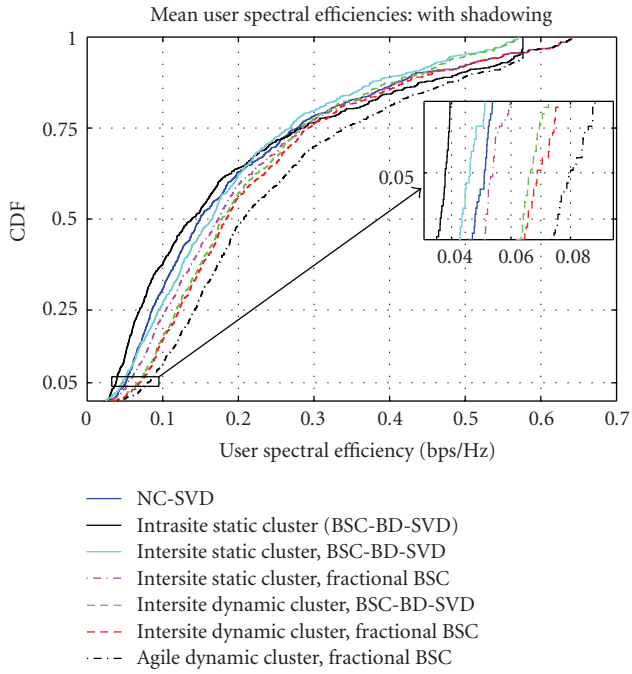

Figure 7: CDF of mean user spectral efficiencies. With shadow fading, intersite distance of 500 meters. 10 UEs per BS.

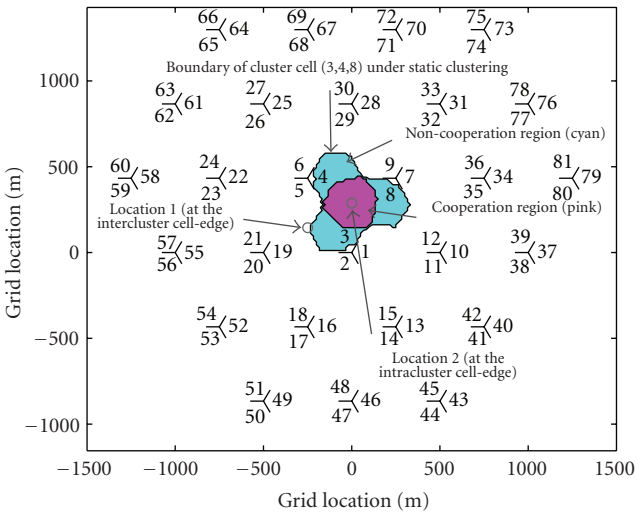

Figure 8: BS site locations and cluster locations of Cluster (3,4,8) under static Clustering no shadow fading. The tri-start represents site locations with its corresponding BS numbers. Intersite distance is 500 meters.

pathloss from the cooperative BSs offset their contribution to capacity. Therefore, at the intercluster cell-edge, BSC-BD-SVD did not provide cooperative gain. For this case, coverage was not improved at the intercluster cell-edge by cooperation.

In Location 2, the gain of BSC-BD-SVD was realized at all intersite distances. However, above the crossover distance $\gamma_{\mathrm{x}}^{\mathrm{Loc2}} = 4208$ meters, the gain was negligible, as shown in Figure 12. If the spectral efficiency requirement $\overline{R}_{\mathrm{STR}}$ is greater than the spectral efficiency of Location 2 at the crossover distance ($\overline{R}_{\mathrm{x}}^{\mathrm{Loc2}}$), then for the test network, cooperation increases the spectral efficiency coverage at the intracluster cell-edge.

It is also observed in Figure 12 that saturation of throughput under BSC-BD-SVD occured at a lower range of intersite distances ($\gamma_{\mathrm{site}} < 600$) compared to that of NC-SVD. This was because the saturation in BSC-BD-SVD was only due to the intercluster interference. Because there is less cochannel interference, cooperation encouraged smaller cell sizes or higher transmit powers to achieve gains in the intracluster cell-edge. By encouraging higher transmit powers given the same site location, cooperation also increased the signal power coverage $\mathbb{V}_{\mathrm{SP}}$ since higher receive signal powers can be achieved. If dynamic clustering is performed for a UE at Location 1, BSs 3, 5, and 19 form the cluster, and the receive signal strength profile and its spectral efficiency will improve to around the same as those of a UE in Location 2, where the BSs which induce the strongest signals cooperate. This shows that dynamic clustering potentially increases the spectral efficiency coverage over static clustering, which must be considered during network dimensioning.

In real networks, shadow fading reduces the lowest spectral efficiency values, as shown in Figure 7. In order to assess the coverage under shadowing, the spectral efficiency CDF may be used to predict coverage. For example, under no shadowing, fractional BSC with dynamic clustering may achieve a 5% cell-edge spectral efficiency of 0.1 bps/Hz/user, while NC-SVD has a lower 5% cell-edge spectral efficiency. Therefore, at a threshold of 0.1 bps/Hz, fractional BSC with dynamic clustering achieves higher spectral efficiency coverage. Through dynamic clustering, the intercluster cell-edge was reduced, as shown in Figure 10, where Location 1 was no longer included in the cell cluster.

Figure 13 shows the spectral efficiency coverages at a threshold of $\overline{R}_{\mathrm{A,STR}} = 1$ bps/Hz (for relatively high guaranteed bit-rate applications). It is observed that under static clustering, BSC-BD-SVD coverage was lower than NC-SVD, and that even with dynamic clustering, the gain was limited in the low-to-medium intersite distances. Therefore, even with dynamic clustering, but without fractional BSC, the gain in spectral efficiency coverage is not guaranteed for all site geometries and intersite distances since the loss of BSC-BD-SVD at the intercluster cell-edge may still offset its gain in the intracluster cell-edge. At larger intersite distances, the system became more noise limited, and the gain of cooperation at the cell-edge was reduced, which reduced the coverage. Therefore, fractional BSC was required to ensure an enhancement of the spectral efficiency coverage $\mathbb{V}_{\mathrm{SE}}$ over NC transmission. It is also shown that under static clustering, intersite clustering achieved greater coverage than intrasite clustering, which correlates to the higher cooperation region area of intersite as shown in Figure 11.

5.2. BSC Impact on Cell Traffic. The cell traffic of BS b of cluster k is given by $\Gamma_{b_k} = \sum_{u=u_{[b_k]}}^{u_{[b_k]}+U_{b_k}-1} \overline{R}_u W_u$, where $u_{[b_k]}$ is the 1st UE of BS b_k, and W_u is the allocated bandwidth of UE u. This reveals that higher mean user spectral efficiencies

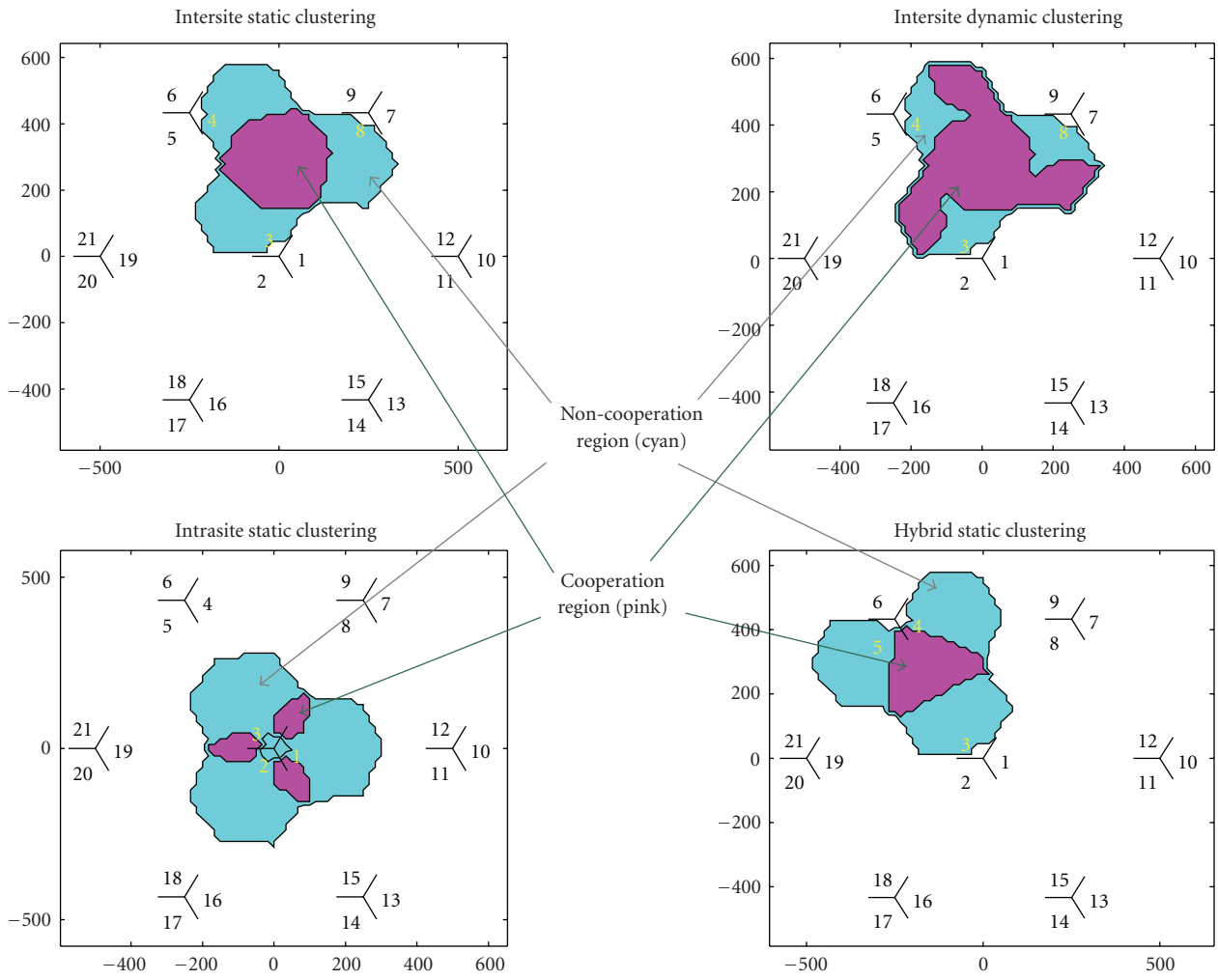

Figure 9: Cluster cells and cell regions under various BSC cluster types. Intersite distance is 500 meters, no shadowing.

directly translates to higher cell traffic. Therefore, the cell-average spectral efficiencies, as shown in Figure 13, reveal how BSC impacts cell traffic. For the example network, BSC-BD-SVD under static clustering failed to increase the cell-average spectral efficiency. But by introducing dynamic clustering, gains over NC-SVD were achieved for smaller intersite distance. Under fractional BSC, the gains existed regardless of the intersite distance. It is observed that the spectral efficiency gains of the various cooperative network types decreased with increasing intersite distance, where spectral efficiency was determined by the LNR. This shows that cooperation encouraged smaller intersite distances or higher transmit powers to achieve gains in cell traffic over NC.

Under intrasite static clustering, the 3-BS cooperation was not effective because the received signal from at least one of the cooperating BSs was usually much lower than that of the local BS. Hence, those weaker signals had insignificant contribution to spectral efficiency. For intrasite cooperation, the spectral efficiency of 2-BS dynamic clustering may perform better than 3-BS static clustering, but this is subject to further study.

Because of the intercluster interference, the traffic gains of cooperation was limited. For this case, the maximum gain was around 26%, which was achieved at low intersite distances. To decrease the intercluster interference, the number of cooperative BSs per cluster may be increased. However, practically, this requires more overhead for coordination.

5.3. BSC Impact on Handover. Under BSC, handover is defined as the switching of a UE from one local BS to another local BS, where the rights to govern the transmission to the UE is passed. Handover is performed by a local BS to an available nearby BS which produces sufficient signal power L_b to a UE at the cell-edge $\mathcal{E}$. To perform handover, both the passing BS and the receiving BS need to have signal strength coverage on the UE location.

In non-cooperative OFDM-based radio interfaces, hard handover is performed since the former local BS needs to "switch off" first before the resource is assigned to the new local BS. However, when joint transmission is performed, under the cluster member handover, a kind of *softer handover* (handover with macro diversity) can be performed even

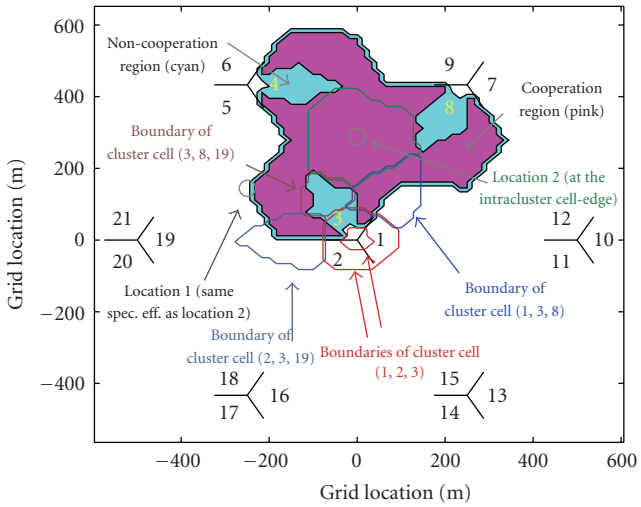

Figure 10: BS site locations and cluster locations of Cells 3,4,8 under agile dynamic clustering and no shadow fading. Intersite distance is 500 meters.

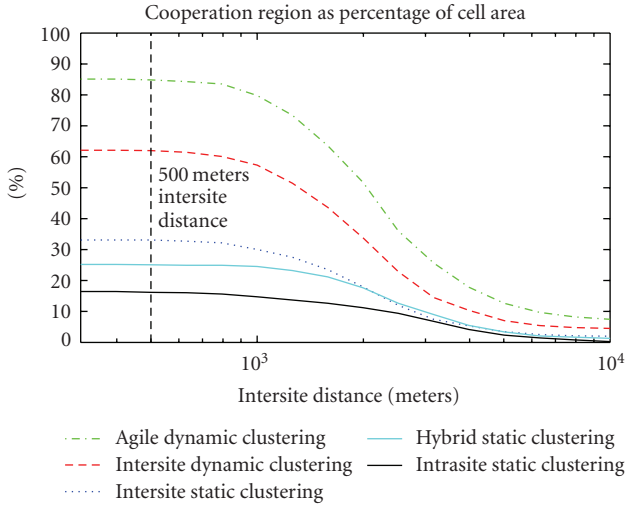

Figure 11: Ratio of cooperation region area to cell region area versus intersite distance. With shadowing.

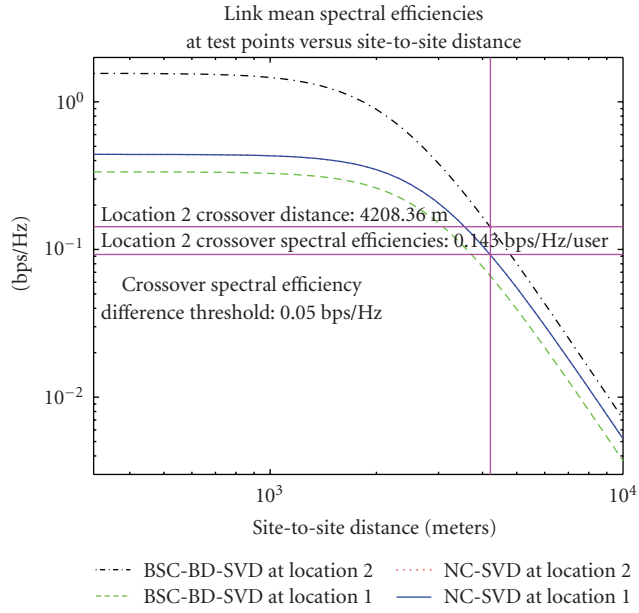

Figure 12: Link mean spectral efficiencies at test locations versus intersite distance. No shadowing. 1 UE per BS.

with OFDM transmission since multiple links are made. The handover procedure may be used to reassign dynamic clusters. Since there is multicoverage, every time handover is executed, the BSs performing handover may form a new dynamic cluster for the UE. The member which produces the weakest signal is simply replaced by the new BS with a stronger received signal. This is called *cluster member handover*. This process is similar to *coffin-passing*, where several pallbearers need to carry the coffin while others take turns. In Shinto tradition, cluster member handover is similar to the process of substitution of carriers of a portable shrine called *mikoshi* during a festival.

When performing cluster member handover, the transmission rates can be kept high since the ongoing members can continue with the cooperative transmission while the weakest member is replaced. This leads to less handover failures since multiple other BSs continue to serve the UE even if one link fails. Moreover, since the BSs which produce the strongest signals remain in cooperation, the BS remains in the intracluster cell-edge, and significant spectral efficiency gains of cooperation are achieved. The previous sections on coverage and traffic show that useful gains in coverage and cell traffic are obtained through BSC at smaller cell sizes or higher transmit powers. Stronger transmit powers mean greater overlap of coverage areas of the BSs. Consequently, because of the overlap of coverage, BSC leads to a greater area where handover can be made.

5.4. BSC Impact on Cost and Complexity. The increased throughputs under BSC come at the expense of increased complexity of the network due to possible additional operations such as wireless feedback of implicit or explicit multicell channel state information (CSI), sharing of CSI and related parameters between BSs, high-speed sharing of data and overhead between BSs, subframe-level or symbol-level multiple BS synchronization, distributed cooperative precoding or decoding, cooperative power control, and cooperative scheduling. The system complexity increases considerably as the number of BSs within a BSC cluster increases.

In performing joint processing, high-speed sharing of data and overhead requires very fast and low-latency intersite backhaul interconnections. Optical communication solutions are being proposed for such purpose, which increases the capital outlay for new BSs. As discussed in the previous sections, the spectral efficiency gain of BSC is more evident for interference-limited situations. Typically, these are in urban microcell and picocell environments in urban areas. With the advent of remote radio heads (RRHs) with extended optical links (>10 km), the baseband units can be colocated in the central urban area, and the backhaul interconnections

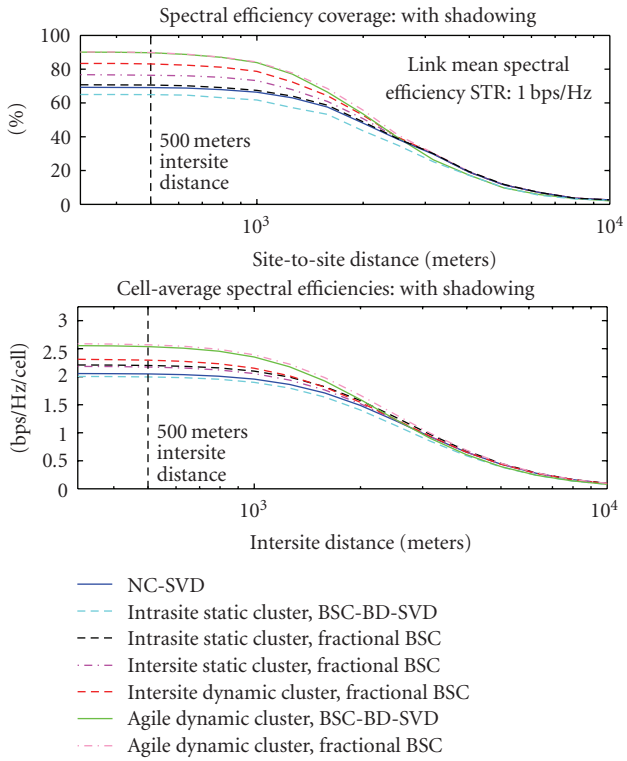

Figure 13: Spectral efficiency coverage and cell-average spectral efficiencies under shadow fading. 10 UEs per BS.

can be in-site. Consequently, additional hardware costs to perform BSC are reduced.

Figure 13 shows that under BSC, the coverages and average spectral efficiencies saturate at small intersite distances. This results in a range of cost-effective intersite distances for BSC under particular channel models and cell topologies. Furthermore, the coverage and traffic gains of BSC over NC for the network are moderate at best. Therefore, only slight to moderate increases in cost are tolerated.

Dynamic clustering introduces further complexity to the scheduler, since the scheduler must not only decide which users are served, but also decide which BSs should cooperate at a given resource. Furthermore, the scheduler must intelligently allocate resources for either cooperation or noncooperation.

6. BSC Impact on Cell Planning Procedure

BSC requires additional procedures to cell planning. First, the question of whether to use NC or BSC for each BS must be decided based on cost-effectiveness. The proportion of additional expense of BSC must not overcome its gain in revenue brought by increased cell traffic. Second, under fractional BSC, the service area must be partitioned into cooperation regions and noncooperation regions in order to accurately estimate the cell traffic serving capability. The size and density of the regions determines the radio resources allocated for cooperation or noncooperation and the required bandwidth of the backhaul.

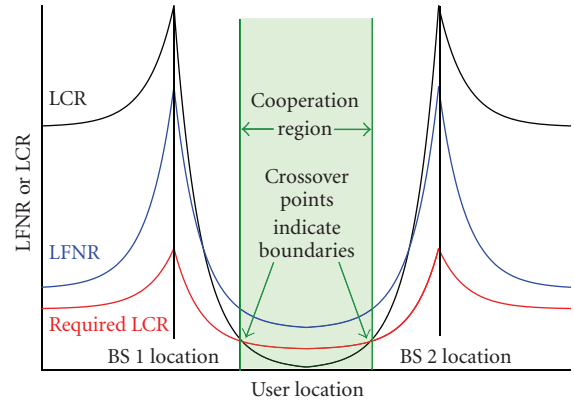

Figure 14: Cell region partitioning.

The cell region partitioning can be performed through the following procedure, as illustrated in Figure 14. First, a map of LUNR and LCR of each location is generated. Then, a maximum LCR threshold may be set for each LUNR. For example, the threshold is the boundary between the cooperation region and noncooperation region in Figure 5. When the LCR is below the LCR threshold, the location is assigned to the cooperative region.

6.1. Cell Plan Analysis Using Receive Signal Strength Ratios. The CDFs of the LNR, LUR, and LCR, as illustrated Figure 4, provide the designer a visual and intuitive approach in the design of the BSC or fractional BSC network. To increase the performance, the design goals are to increase the LNRs and LURs, and to control the LCRs. Under joint transmission and joint processing, the goal is to decrease the LCRs or increase the concentration of UEs around the low-LCR region. A two-dimensional distribution of the LUNRs and LCRs at UE locations, mapped to a spectral efficiency table such as in Figure 5, allows the designer to predict and compare the coverage and traffic performance of tentative network designs.

In summary of the results, it was observed that if the geometry is maintained, the LCRs and LURs do not change with respect to intersite distance. In addition, at low intersite distances, the LNR is too high to have an impact on the traffic and coverage. Therefore, at low intersite distances, the CDFs of the LCRs and LURs determine the upper-bound gains of BSC. At high intersite distances, the noise becomes dominant over LCR, which forces the performance of BSC networks to approach that of NC.

6.2. BS Positioning and Clustering Optimization under BSC. The spectral efficiency coverage optimization problem in Section 5.1 requires the calculation of each node's estimated spectral efficiency at each STP. This involves estimating the LUNR and LCR generated from the link budget of each base station configuration. A simpler heuristic approach is to formulate the problem as an integer program of selecting a limited number of sites or configurations [15, 22] from a total of N_L candidate site locations or configurations based

only on the resulting LNRs. Such problem is NP-hard, but efficient polynomial time near-optimal solutions exist [22, 23]. Mathematically, the problem is to select the set of $\beta_l \in \{0,1\}$, $l = 1,\ldots,N_{\mathrm{L}}$, where $\beta_l = 1$ represents the existence of a base station in site l, and 0 otherwise.

The fundamental BS positioning problem is the maximum signal coverage location problem, where the area of signal coverage is maximized given a budget for the number of sites. The signal coverages are represented by $\mathbf{C} \in \{0,1\}^{N_S \times N_{\mathrm{L}}}$, with element $c_{s,1} = 1$ if $\mathrm{LNR}_{(s),l} \geq \mathrm{LNR}_{\mathrm{cov}}$, and 0 otherwise.

Maximum Signal Coverage Location Problem (MSCLP). It holds that

$$\text{maximize} \quad \mathbb{V}_{\mathrm{cov}} \tag{15}$$

$$\text{such that} \quad \mathbb{V}_{\mathrm{cov}} = \sum_{s=1}^{N_S} z_s \tag{16}$$

$$\sum_{l=1}^{N_{\mathrm{L}}} \beta_l \leq N_{\mathrm{B}}^{\mathrm{budget}} \tag{17}$$

$$z_s = \begin{cases} 1 & \displaystyle\sum_{l=1}^{N_{\mathrm{L}}} \beta_l c_{s,l} \geq 0 \\ 0 & \text{otherwise,} \end{cases} \tag{18}$$

where $N_{\mathrm{B}}^{\mathrm{budget}}$ is the budget for the number of BSs.

The MSCLP does not consider multiple coverage, that is, overlap of the signal coverage. However, in non-cooperative single-frequency networks, multiple coverages are discouraged since they lead to excessive interference. Moreover, under BSC, multiple coverage of cooperating base stations are penalized less than the multiple coverage of non-cooperating base stations. By intelligently penalizing multiple coverage, the MSCLP can be extended as follows for BSC.

MSCLP with Multiple Coverage Penalties under BSC (MCPBSC). It holds that

$$\text{maximize} \quad \mathbb{V}_{\mathrm{cov}} - \mu \mathbb{V}_{\mathrm{mcov}} \tag{19}$$

$$\text{such that} \quad (16)\text{–}(18) \text{ hold} \tag{20}$$

$$\mathbb{V}_{\mathrm{mcov}} = \sum_{l=1}^{N_{\mathrm{L}}} \sum_{k>l}^{N_{\mathrm{L}}} \beta_l \beta_k w_{l,k} \sum_{s=1}^{N_S} c_{s,l} c_{s,k} \tag{21}$$

$$w_{l,k} = \begin{cases} w_{\mathrm{NC}} & \text{BSs at location } l \text{ and } k \text{ are noncooperative} \\ w_{\mathrm{C}} & \text{BSs at location } l \text{ and } k \text{ are cooperative,} \end{cases} \tag{22}$$

where μ ($0 \leq \mu$) is a weighing factor to control the influence of the multiple coverage on the optimization. The penalty weights are w_{NC} for multicoverage of non-cooperative BSs and w_{C} for multicoverage within a BS cluster, where $0 < w_{\mathrm{NC}} < 1$ and $w_{\mathrm{C}} < w_{\mathrm{NC}}$. Under joint processing BSC, multiple coverage can even be encouraged since it leads to a reduction in LCR and consequently increased spectral efficiency. Therefore, under joint processing BSC, $w_{\mathrm{C}} < 0$.

As discussed in Section 5.1, coverage can be extended by BSC at the intracluster cell-edge. This is reflected in the following optimization problem.

MSCLP with MCPBSC and Intracluster Coverage Extension (ICE). It holds that

$$\begin{aligned} &\text{maximize} \quad \mathbb{V}_{\mathrm{cov}} - \mu \mathbb{V}_{\mathrm{mcov}} + \xi \mathbb{V}_{\mathrm{ecov}} \\ &\text{such that} \quad (16)\text{–}(18), (21)\text{-}(22) \text{ hold} \\ &\mathbb{V}_{\mathrm{ecov}} = \sum_{l=1}^{N_{\mathrm{L}}} \sum_{k>l}^{N_{\mathrm{L}}} \cdots \sum_{i>k}^{N_{\mathrm{L}}} \beta_l \beta_k \ldots \beta_i w_{l,k,\ldots,i} \\ &\qquad \times \sum_{s=1}^{N_S} c_{s,l}^{(\mathrm{e})} c_{s,k}^{(\mathrm{e})} c_{s,i}^{(\mathrm{e})} m_{s,l,k,\ldots,i}, \end{aligned} \tag{23}$$

where ξ ($\xi \geq 0$) is a weighing factor to control the influence of the extended coverage on the optimization, and

$$w_{l,k,\ldots,i} = \begin{cases} 1 & \text{BSs at sites } l,k,\ldots,i \text{ form a BSC cluster} \\ 0 & \text{otherwise,} \end{cases}$$

$$c_{s,l}^{(\mathrm{e})} = \begin{cases} 1 & \mathrm{LNR}_{(s),l} \geq \mathrm{LNR}_{\mathrm{cov}}^{(\mathrm{e})} \\ 0 & \text{otherwise,} \end{cases}$$

$$m_{s,l,k,\ldots,i} = \begin{cases} 0 & \displaystyle\sum_{\substack{n=1 \\ n \neq l,k,\ldots,i \\ w_{l,n}=0 \\ w_{k,n}=0 \\ \vdots \\ w_{i,n}=0}}^{N_{\mathrm{L}}} \beta_n c_{s,n} \geq 0 \\ 1 & \text{otherwise.} \end{cases} \tag{24}$$

Extended signal coverage from site l to STP s is given by $c_{s,l}^{(\mathrm{e})}$. $\mathrm{LNR}_{\mathrm{cov}}^{(\mathrm{e})}$ is the LNR required for the extended signal coverage, where $\mathrm{LNR}_{\mathrm{cov}}^{(\mathrm{e})} \leq \mathrm{LNR}_{\mathrm{cov}}$. In the presence of the interference from a non-cooperative BS at the extended coverage location, $m_{l,k,\ldots,i,s} = 0$, which nullifies the extended coverage at that location.

Studies related to solving for the weighing factors μ and ξ and the integer programming algorithms are beyond the scope of this paper.

6.2.1. Cardinality of the MSCLP and Its Extensions. Without BSC, the cardinality of the MSCLP and its extensions is

$$|\mathcal{P}_{\mathrm{NC}}| = \sum_{n=1}^{n=N_{\mathrm{B}}^{\mathrm{budget}}} {}_{N_{\mathrm{L}}}\mathrm{C}_n. \tag{25}$$

Under BSC with static clustering clustering, the clusters must be selected for each candidate set of sites. Assuming $N_{\mathrm{C}} \leq N_{\mathrm{B}}^{\mathrm{budget}}$, the cardinality becomes

$$|\mathcal{P}_{\mathrm{SC}}| = \sum_{n=1}^{n=N_{\mathrm{C}}} {}_{N_{\mathrm{L}}}\mathrm{C}_n + \sum_{m=N_{\mathrm{C}}+1}^{m=N_{\mathrm{B}}^{\mathrm{budget}}} \left(\left({}_{N_{\mathrm{L}}}\mathrm{C}_m \right) \prod_{p=1}^{N_{\mathrm{B}}^{\mathrm{budget}}/N_{\mathrm{C}}} \left({}_{m-(p-1)N_{\mathrm{C}}}\mathrm{C}_{N_{\mathrm{C}}} \right) \right). \tag{26}$$

The right-side factors of the second summation term of (26) refer to the possible cluster combinations once the candidate sites are selected. Indeed, under BSC, the selection of the BSC clusters, as indicated by the selection of $w_{l,k,\ldots,i}$s, is part of the planning, thereby increasing the cardinality. Fortunately, only BSs at nearby site locations allow for low LCR regions or overlapping intracluster coverages. Therefore, in practical scenarios, the BSC clusters can be limited to those having nearby members, and the cardinality can be more limited.

Under BSC with dynamic clustering, each BS can form clusters with any of its neighbors. Therefore, the clustering need not be planned and the cardinality of the planning problem is

$$|\mathcal{P}_{\mathrm{DC}}| = \sum_{n=1}^{n=N_{\mathrm{B}}^{\mathrm{budget}}} {}_{N_{\mathrm{L}}}\mathrm{C}_n, \tag{27}$$

which is the same as that of noncooperation.

6.2.2. Illustrative Example. To illustrate the concepts, consider the following MSCLP-MCPBSC-ICE example in Figure 15 with the following parameters: $\mu = \xi = w_{\mathrm{NC}} = 1$, and $w_{\mathrm{C}} = 0$. These mean that multicoverage among two non-cooperating BSs cancels the single coverage, and multicoverage among two cooperating BSs does not cancel the coverage. The objective then is to maximize the effective number of covered STPs given $N_{\mathrm{B}}^{\mathrm{budget}} = 4$ and BSC static clustering with $N_{\mathrm{C}} = 3$. The optimum solution is found to be sites $\{1, 2, 3, 5\}$ with static Cluster (1,2,3), which yields a coverage of 9 STPs (all except STP 9).

For the example problem, only a single cluster is possible since $N_{\mathrm{B}}^{\mathrm{budget}} \leq 2N_{\mathrm{C}}$. Hence, there is only a single term in the $\prod$ expression of (26), which is ${}_4\mathrm{C}_3$. This allows for a solution by manual inspection, since the cardinality for noncooperation case is 50, and for cooperation, 65. Otherwise, the cardinality quickly increases since clusters must also be selected for the rest of the yet-to-be-clustered candidate sites.

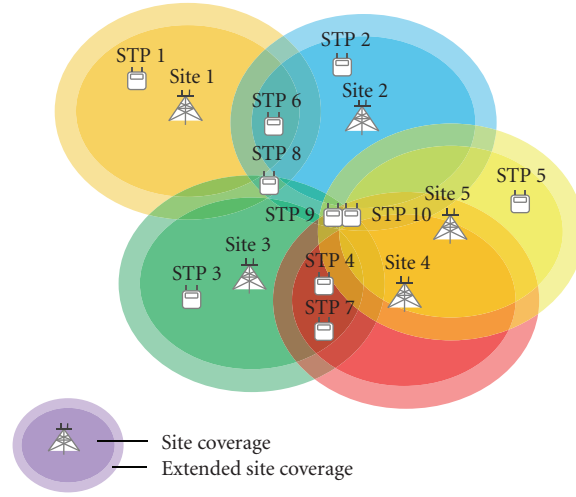

Figure 15: Illustrative example of a BS positioning and clustering optimization problem under BSC.

7. Conclusion and Recommendation

Base station cooperation (BSC) enables better cellular network performance but introduces new challenges to network operation. In this paper, we have discussed various ways on how BSC impacts cell planning. To estimate the performance of a BSC network, the spectral efficiency of a UE was estimated based on the received signal strength ratios of the local BS, cooperative BSs, and uncooperative BSs. The cooperative base station clusters were formed and the impact of the interference from the other clusters was assessed.

Our simulation results have shown that locations in a cell exist where non-cooperative (NC) transmission yields higher spectral efficiency than block-diagonalization, which is a form of joint-transmission BSC. Hence, a network which performs a specific BSC scheme to all its UEs may achieve lower cell-edge or lower cell-average spectral efficiencies. It is proposed that fractional BSC operation be performed with dynamic clustering of BS cells based on the received signal strengths to ensure gains regardless of the topology. The simulation results also suggest that BSC maximizes its gains over NC in a network where the signal strengths from cooperative BSs are close to that of the local cell (i.e., at the intracluster cell-edge). This encourages smaller cell sizes and higher transmit powers. Because of the interference from the intercluster BSs, the gains of BSC are upper bounded, and diminishes at greater intersite distances because of noise. Higher transmit powers produces greater overlap of coverage, which increases the area available for handover. Since the gains of BSC are upper bounded and are typically moderate (for a hexagonal layout of 3-sector BS sites with 3-BS cluster size), the additional costs of BSC must also be moderate.

We have also shown that the BSC cluster type and its reconfigurability (static or dynamic) affects the cell area coverage given a certain site-to-site distance. Therefore, these must also be considered in network dimensioning, where

site-to-site distance is determined to guarantee a minimum cell area coverage or maximum cell outage probability. In addition, the selection of static BSC clusters increases the cardinality of cell planning optimization problem.

The discussed methods and additional cell plan procedures can be extended to more sophisticated transmission schemes and other site geometries for use in practical networks. In our analysis, it was assumed that each BS is uncapacitated, that is, it can support an unlimited number of UEs and has no maximum limit to total capacity. Therefore, user throughputs solely determined the selection of the BS cluster in dynamic clustering, and load balancing was not investigated. The impact of cooperative load balancing to cell planning is a topic for future study.

References

[1] P. Marsch and G. Fettweis, "On base station cooperation schemes for downlink network MIMO under a constrained backhaul," in *Proceedings of IEEE Globecom Workshops (GLOBECOM '08)*, pp. 1219–1224, New Orleans, La, USA, November-December 2008.

[2] L. Ping, P. Wang, H. Wang, and X. Lin, "On cellular capacity with base station cooperation," in *Proceedings of IEEE Globecom Workshops (GLOBECOM '08)*, pp. 3761–3765, New Orleans, La, USA, November-December 2008.

[3] S. Shamai and B. M. Zaidel, "Enhancing the cellular downlink capacity via co-processing at the transmitting end," in *Proceedings of the 53rd IEEE Vehicular Technology Conference (VTC '01)*, pp. 1745–1749, Rhodes, Greece, May 2001.

[4] H. Zhang and H. Dai, "Cochannel interference mitigation and cooperative processing in downlink multicell multiuser MIMO networks," *EURASIP Journal on Wireless Communications and Networking*, vol. 2004, no. 2, pp. 222–235, 2004.

[5] S. Jing, D. N. C. Tse, J. Hou, J. B. Soriaga, J. E. Smee, and R. Padovani, "Multi-cell downlink capacity with coordinated processing," in *Proceedings of the Information Theory and Application Workshop (ITA '07)*, San Diego Calif, USA, January 2007.

[6] M. K. Karakayali, G. J. Foschini, R. A. Valenzuelat, and R. D. Yates, "On the maximum common rate achievable in a coordinated network," in *Proceedings of IEEE International Conference on Communications (ICC '06)*, pp. 4333–4338, Istanbul, Turkey, June 2006.

[7] H. Dahrouj and W. Yu, "Coordinated beamforming for the multi-cell multi-antenna wireless system," in *Proceedings of the 42nd Annual Conference on Information Sciences and Systems (CISS '08)*, pp. 429–434, Princeton, NJ, USA, March 2008.

[8] S. Venkatesan, A. Lozano, and R. Valenzuela, "Network MIMO: overcoming intercell interference in indoor wireless systems," in *Proceedings of the 41st Asilomar Conference on Signals, Systems and Computers (ACSSC '07)*, pp. 83–87, Pacific Grove, Calif, USA, November 2007.

[9] S. Ramprashad and G. Caire, "Cellular vs. network MIMO: a comparison including channel state information," in *Proceedings of the 20th IEEE International Symposium on Personal, Indoor and Mobile Radio Communications (PIMRC '09)*, Tokyo, Japan, September 2009.

[10] 3GPP TSG-RAN, "Further Advancements for E-UTRA; Physical Layer Aspects (Release 9)," 3GPP Std. TR 36.814 v.0.4.1, 2009.

[11] Philips Electronics, "Multi-cell co-operative beamforming: TP for TR 36.814," 3GPP Std, Temporary Document R1-091 720, 2009.

[12] D. Amzallag, M. Livschitz, J. Naor, and D. Raz, "Cell planning of 4G cellular networks: algorithmic techniques and results," in *Proceedings of the 6th International Conference on 3G 3G and Beyond*, pp. 1–5, Washington, DC, USA, 2005.

[13] S. Hurley, "Planning effective cellular mobile radio networks," *IEEE Transactions on Vehicular Technology*, vol. 51, no. 2, pp. 243–253, 2002.

[14] H. Son and S. Lee, "The cell planning scheme for ICI mitigation," in *Proceedings of the 18th IEEE International Symposium on Personal, Indoor and Mobile Radio Communications (PIMRC '07)*, Athens, Greece, September 2007.

[15] R. Mathar and T. Niessen, "Optimum positioning of base stations for cellular radio networks," *Wireless Networks*, vol. 6, no. 6, pp. 421–428, 2000.

[16] R. M. Whitaker and S. Hurley, "Evolution of planning for wireless communication systems," in *Proceedings of the 36th Annual Hawaii International Conference on System Sciences (HICSS '03)—Track 9*, pp. 296–305, IEEE Computer Society, Washington, DC, USA, 2003.

[17] S. Allen, B. Belloul, S. Hurley, S. Saunders, and R. M. Whitaker, "Smart cell planning and optimisation for UMTS," in *Proceedings of the 5th International Conference on 3G Mobile Communication Technologies*, pp. 34–38, London, UK, 2004.

[18] I. D. Garcia, K. Sakaguchi, and K. Araki, "Cell planning for cooperative transmission," in *Proceedings of IEEE Wireless Communications and Networking Conference (WCNC '08)*, pp. 1769–1774, Las Vegas, Nev, USA, March-April 2008.

[19] I. Garcia, K. Sakaguchi, N. Kusashima, K. Araki, S. Kaneko, and T. Inoue, "Cell planning of fractional base station cooperation network based on MIMO channel model," Tech. Rep. AP2008-233, IEICE, March 2009.

[20] 3GPP TSG-RAN1 (LTE-Advanced Rapporteur), "Overhead assumption for performance evaluation for ITU submission," 3GPP Std. Temporary Document R1-093 611, 2009.

[21] P. Mogensen, W. Na, I. Z. Kováes et al., "LTE capacity compared to the shannon bound," in *Proceedings of the 65th IEEE Vehicular Technology Conference (VTC '07)*, pp. 1234–1238, Dublin, Ireland, April 2007.

[22] C. Glaßer, S. Reith, and H. Vollmer, "The complexity of base station positioning in cellular networks," *Discrete Applied Mathematics*, vol. 148, no. 1, pp. 1–12, 2005.

[23] N. Megiddo, E. Zemel, and S. L. Hakimi, "The maximum coverage location problem," *SIAM Journal on Algebraic and Discrete Methods*, vol. 4, no. 2, pp. 253–261, 1983.